HHS Public Access

Author manuscript

Brain Behav Immun. Author manuscript; available in PMC 2017 August 28.

Published in final edited form as:

Brain Behav Immun. 2017 August ; 64: 344–353. doi:10.1016/j.bbi.2017.04.019.

Using functional and molecular MRI techniques to detect neuroinflammation and neuroprotection after traumatic brain injury

Wenzhu Wang[a,b,1], **Hong Zhang**[c,d,1], **Doon-Hoon Lee**[c], **Jintao Yu**[e], **Tian Cheng**[a], **Michael Hong**[a], **Shanshan Jiang**[c], **Heng Fan**[b], **Xi Huang**[f,g,2,3], **Jinyuan Zhou**[c,2,4], and **Jian Wang**[a,2,*]

[a]Department of Anesthesiology and Critical Care Medicine, Johns Hopkins University School of Medicine, Baltimore, MD 21205, USA

[b]Department of Integrated Chinese and Western Medicine, Union Hospital, Tongji Medical College, Huazhong University of Science and Technology, Wuhan 430022, Hubei, China

[c]Division of MR Research, Department of Radiology, Johns Hopkins University School of Medicine, Baltimore, MD 21287, USA

[d]Department of Radiology, Beijing Children's Hospital, Capital Medical University, Beijing 100045, China

[e]Department of Otorhinolaryngology, Union Hospital, Tongji Medical College, Huazhong University of Science and Technology, Wuhan 430022, Hubei, China

[f]Gerontology Department, Affiliated Hospital of Nanjing University of Chinese Medicine, Nanjing 210029, Jiangsu, China

[g]Institute of TCM-Related Comorbid Depression, Nanjing University of Chinese Medicine, 138 Xianling Road, Nanjing 210046, Jiangsu, China

Abstract

This study was designed to investigate whether functional and molecular MRI techniques are sensitive biomarkers for assessment of neuroinflammation and drug efficacy after traumatic brain injury (TBI) in rats. We subjected rats to a controlled cortical impact model and used behavioral tests, histology, and immunofluorescence to assess whether flavonoid pinocembrin provides cerebral protection and improves functional recovery. Most importantly, we used multiple noninvasive structural, functional, and molecular MRI techniques to examine whether the pinocembrin-related neuroprotection and attenuation of neuroinflammation can be detected *in*

[*]Corresponding author at: Department of Anesthesiology and Critical Care Medicine, Johns Hopkins University School of Medicine, 720 Rutland Ave, Ross Bldg 370B, Baltimore, MD 21205, USA.

[1]These authors contributed equally to this work.

[2]These authors jointly supervised this work.

[3]Institute of TCM-Related Depressive Comorbidity, Nanjing University of Traditional Chinese Medicine, 138 Xianling Road, Nanjing 210064, Jiangsu, China.

[4]Division of MR Research, Department of Radiology, Johns Hopkins University, 600 N. Wolfe Street, Park 336, Baltimore, MD 21287, USA.

Conflict of interest

Dr. Jinyuan Zhou is co-inventor on a patent for the APT MRI technology. This patent is owned and managed by Johns Hopkins University. All other authors declare no competing financial interests.

vivo. Significant increases in cerebral blood flow (CBF) and amide proton transfer-weighted (APTw) MRI signals were observed in the perilesional areas in untreated TBI rats at 3 days and could be attributed to increased glial response. In addition, increased apparent diffusion coefficient and decreased magnetization transfer ratio signals in untreated TBI rats over time were likely due to edema. Post-treatment with pinocembrin decreased microglial/macrophage activation at 3 days, consistent with the recovery of CBF and APTw MRI signals in regions of secondary injury. These findings suggest that pinocembrin provides cerebral protection for TBI and that multiple MRI signals, CBF and APTw in particular, are sensitive biomarkers for identification and assessment of neuroinflammation and drug efficacy in the TBI model.

Keywords

APT imaging; Flavonoid; Molecular imaging; MRI; Neuroinflammation; Neuroprotection; Traumatic brain injury

1. Introduction

Traumatic brain injury (TBI) is a serious public health problem that affects an estimated 1.7 million Americans annually (CDC statistics, 2010). It is a complex injury that results in primary injury and secondary injury cascades. Variable outcomes of patients after TBI and the multiple definitions of TBI make interpreting results across research studies challenging (Amyot et al., 2015). Currently, no drug is effective for treatment of TBI, and clinical trials of neuroprotective drugs have not shown clear benefit in reducing or preventing secondary brain damage (McConeghy et al., 2012). Therefore, it is imperative to develop an effective treatment for TBI.

Pinocembrin (5,7-dihydroxyflavanone) is a natural flavonoid compound extracted from honey, propolis, ginger root, wild marjoram, and other plants (Lan et al., 2016; Rasul et al., 2013). In the last few years, preclinical studies have shown that it has antiinflammatory (Lan et al., 2017; Saad et al., 2015) and neuroprotective effects (Kapoor, 2013; Wang et al., 2016b), as well as the ability to reduce reactive oxygen species (Wang et al., 2016b), protect the neurovascular unit (Liu et al., 2014), and modulate mitochondrial function (de Oliveira et al., 2016). It can also regulate apoptosis (Saad et al., 2015; Wu et al., 2013), detoxification, and immunity genes (Mao et al., 2013). The pharmacokinetics and pharmacodynamics of pinocembrin recently have been reported in rats (Sayre et al., 2015) and in humans (Cao et al., 2015; Yan et al., 2014). Furthermore, pinocembrin has been authorized by the State Food and Drug Administration of China for clinical trials in patients with ischemic stroke, and phase II trials have begun (ClinicalTrials.gov Identifier: NCT02059785) (Yan et al., 2014). Nevertheless, its potential efficacy in TBI has not been tested.

The application of neuroimaging techniques, such as magnetic resonance imaging (MRI), has considerably advanced our understanding of various complex neurologic disorders (Yang et al., 2017). Preclinical and clinical data have indicated that MRI is critical for assessing structural and functional changes of TBI that are related to the pathophysiology and clinical manifestations of neurologic disorders (Jaiswal, 2015; Long et al., 2015; Shultz et al., 2015). MRI is commonly used to ascertain measures of structure (T_2 and T_1) and

function (apparent diffusion coefficient [ADC, which measures the diffusion rate of water molecules] and cerebral blood flow [CBF]). Further, scientists are investigating whether molecular MRI techniques can be used to assess some neurologic diseases and their response to therapy (Amyot et al., 2015; Zhou et al., 2003, 2011). For example, it has recently been shown that protein-based amide proton transfer (APT) MRI can accurately detect hyperacute intracerebral hemorrhage and distinctly differentiate intracerebral hemorrhage from cerebral ischemia in rats (Wang et al., 2015). APT imaging is a molecular MRI method that can noninvasively detect endogenous mobile protein concentration and tissue pH changes. In this study, we subjected rats to a controlled cortical impact (CCI) TBI model and used behavioral tests, histology, and immunofluorescence to assess whether pinocembrin provides cerebral protection and improves functional recovery. We also used multiple noninvasive structural, functional, and molecular MRI techniques to examine whether the pinocembrin-related neuroprotection and attenuation of neuroinflammation can be detected *in vivo*.

2. Materials and methods

2.1. Animals

All animal studies were conducted in accordance with National Institutes of Health guidelines and were approved by the Johns Hopkins University Animal Care and Use Committee. Forty-one adult, male Sprague-Dawley rats (300–350 g) were obtained from Charles River Laboratories (Frederick, MD) and maintained in the Johns Hopkins animal facility. All efforts were made to minimize the numbers of animals used and ensure minimal suffering. Animal experiments were reported in accordance with the ARRIVE (Animal Research: Reporting *In Vivo* Experiments) guidelines (www.nc3rs.org.uk/arrive-guidelines).

2.2. CCI model of TBI

Rats were anesthetized initially with 5% isoflurane and maintained with 1.5%–2% isoflurane in oxygen-enriched air (20% oxygen/ 80% air) with spontaneous ventilation. CCI injury was induced with a PSI TBI-0310 Impactor (Precision Systems and Instrumentation, Fairfax, VA), which uses electromagnetic force to produce an impact velocity for which speed, depth, and dwell time can each be individually manipulated to produce injuries with different severities (Cheng et al., 2016). The rats were placed on a stereotactic frame with a built-in heating bed that maintains body temperature at 37 °C. The head was mounted in the stereotactic frame. Under aseptic conditions, a midline longitudinal incision was made over the skull, and a 5-mm craniotomy was made using a portable drill and trephine over the left parietal cortex (center of the coordinates of the craniotomy relative to bregma: 1 mm posterior, 1 mm lateral). The bone flap was removed. A pneumatic cylinder with a 3-mm flat-tip impounder produced CCI in the rats at a velocity of 5.5 m/s, depth of 5 mm, and impact duration of 65 ms. The scalp was closed with cyanoacrylate tissue glue. Rats of the sham group received a scalp incision, but the skull was kept intact. After they resumed locomotor activity, the rats were returned to their home cages.

2.3. Experimental groups and administration of drugs

Pinocembrin was dissolved in sterile saline. Rats were randomly divided (http://www.randomization.com) (Han et al., 2016) into four groups: sham (5 rats), TBI + vehicle (sterile saline; 20 rats), TBI + pinocembrin 5 mg/kg (11 rats), and TBI + pinocembrin 10 mg/kg (5 rats). An investigator blinded to treatment administered pinocembrin or an equal volume of saline by tail vein injection at 30 min after CCI and again 1, 2, and 3 days post-CCI. Sham rats were administered an equivalent volume of saline at 30 min after craniotomy. We chose the delivery route, dosing, and treatment regimens for pinocembrin based on previous work (Guang and Du, 2006; Meng et al., 2014; Shi et al., 2011; Wu et al., 2013).

2.4. MRI data acquisition

Imaging experiments were performed on a 4.7 T animal MRI system (Bruker Biospin, Billerica, MA) with an actively decoupled cross-coil setup (a 70-mm body coil for radiofrequency transmission and a 25-mm surface coil for signal reception). MRI data were acquired at six time points (within 1 h and 1, 3, 7, 14, and 28 days after TBI). First, axial/coronal T_2w images were acquired with the following parameters: repetition time (TR) = 3 s; echo time (TE) = 64 ms; 5 slices; thickness = 1.5 mm; field of view = 42/32 × 32 mm^2; matrix = 256/192 × 192; number of averages (NA) = 2. Then, several quantitative MRI parameters were acquired with previously described methods, including T_2 (TR = 3 s; TE = 30, 40, 50, 60, 70, 80, and 90 ms; NA = 4), T_1 (inversion recovery; pre-delay = 3 s; TE = 30 ms; inversion recovery times = 0.5, 0.3, 0.6, 1.2, 1.8, 2.5, and 3.5 s; NA = 4), isotropic ADC (TR = 3 s; TE = 80 ms; b-values = 0, 166.7, 333.3, 500, 666.7, 833.3, and 1000 s/mm^2; NA = 8), CBF (arterial spin labeling; 3-s labeling at a distance of 20 mm away from the imaging slice; TR = 6 s; TE = 28.6 ms), APT (frequency-labeling offsets of ±3.5 ppm; TR = 10 s; TE = 30 ms; saturation power = 1.3 μT; saturation time = 4 s; NA = 16), and conventional MTR (with the same experimental parameters as APT, except a saturation frequency offset of 10 ppm, namely, 2000 Hz at 4.7 T).

2.5. Image analysis

All MRI data were processed by using Interactive Data Language V7 (Exelis Visual Information Solutions, Inc., Boulder, CO) and previously described methods (Zhou et al., 2003, 2011). Lesion volumes were measured manually as the sum of all injury voxels in all slices on the high-resolution T_2w images. After being interpolated to 384 × 384, the T_2 map, T_1 map, and ADC map were fitted by using the following equations: $I = I_0 \exp(-TE/T_2)$, $I = A + B \exp(-TI/T_1)$, and $I = I_0 \exp(-b\ ADC)$, respectively. The CBF map was reconstructed from images with and without labeling. The APT-MRI signal was quantified by the MTR asymmetry from images with and without labeling. −r: $MTR_{asym}(3.5\ ppm) = S_{sat}(-3.5\ ppm)/S_0 - S_{sat}(+3.5\ ppm)/S_0$ (where S_{sat} and S_0 are the signal intensities with and without RF irradiation). We obtained the MTR map at an offset of 10 ppm using the equation: $MTR(10\ ppm) = 1 - S_{sat}(10\ ppm)/S_0$. For the quantitative image analysis, the signal abnormalities on the high-resolution T_2w images were used as a reference for defining regions of interest (ROIs): core area, ipsilateral cortex, ipsilateral hippocampus, contralateral cortex, and

contralateral hippocampus. These ROIs were drawn manually on the ADC maps and then transferred to identical sites on other co-registered MRI maps.

2.6. Behavioral testing

2.6.1. Neurologic deficits—An investigator blinded to group evaluated neurologic function before TBI and on days 1, 3, 7, 14, and 28 after TBI with the modified neurologic severity score (mNSS) (Wang et al., 2013a, 2016a). The mNSS is a composite of motor (muscle status and abnormal movement), sensory (visual, tactile, and proprioceptive), reflex, and balance tests. Neurologic function was graded on a scale of 0–18, where 0 is normal and 18 indicates maximal neruologic deficit.

2.6.2. Rotarod—We used the rotarod test to examine motor deficits of rats before TBI, at 1 h post-TBI, and at 1, 3, 7, 14, and 28 days post- TBI. The rotarod device (Rotamex-5; Columbus Instruments) requires the animal to walk on a frame with a motorized rotating assembly of 18 rods (1 mm in diameter). The rotational speed of the device is increased from 0 to 30 rpm (rpm) in intervals of 3 rpm for 10-s periods. The rotarod score was recorded as the duration in seconds at which the animal completed the 2-min task, fell from the rods, or gripped the rods and spun for two consecutive revolutions rather than actively walking (Hamm et al., 1994).

2.6.3. Beam walking test—This test is used to evaluate the rats' ability to traverse a beam. Rats were trained to walk on a wooden beam ($2.5 \times 2.5 \times 80$ cm^3) elevated 60 cm above the floor to return to the goal box. Before CCI, the rats were trained once daily for 3 days. After CCI, the rats were tested at 1 h and at 1, 3, 7, 14, and 28 days. Traversing ability was assessed on a modified scale: 0 = traverses the beam with no foot slip; 1 = traverses while grasping the lateral side of the beam; 2 = shows disability of walking on the beam but can traverse; 3 = takes a considerable amount of time to traverse the beam because of difficulty walking; 4 = unable to traverse the beam; 5 = unable to move the body or any limb on the beam; 6 = unable to stay on the beam for 10 s (Goldstein and Davis, 1990).

2.7. Histology

Rats were anesthetized and underwent intracardiac perfusion with 4% paraformaldehyde in 0.1 mol/L phosphate-buffered saline (pH 7.4). The brains were removed and kept in 4% paraformaldehyde for 48 h before being immersed in 30% sucrose for 3 days at 4 °C. The brains were then cut into 20-μm-thick coronal sections with a cryostat, stained with Cresyl violet (for neurons), and dehydrated in an alcohol and acetone series. Coverslips were placed over the sections and sealed with mounting medium.

2.8. Stereological measurement of absolute neuronal number

Coded slides were used for unbiased stereological analysis to ensure that the investigator was blinded to the treatment groups (Cheng et al., 2016; Yang et al., 2013). We analyzed the surviving neurons in the top half of the cortex in the injured hemisphere (between bregma −0.8 mm and bregma −2.8 mm) with a Nikon Eclipse 600 microscope and quantified them using Stereo Investigator Software (MBF Bioscience, Williston, VT) (Cheng et al., 2016). We used an optical fractionator method to estimate the number of surviving neurons in the

cortex under 40x objective lens. We selected dissector frame areas of 1.4 mm^2 with a guard thickness of 10 μm in every 10 sections. With 9 counting frames sampled per section, the number of neurons counted in each frame was 40–90. A viable neuron could be distinguished from glia based on its size, presence of a visible rim of cytoplasm around the nucleus, and a prominent nucleolus. A neuron was not counted when its nucleus came into focus within the guard zone or if the nucleus was touching the left or bottom side of the dissector frame. The mean section thickness, measured at every counting frame site, was used for final calculation of the number of surviving neurons in the cortex. A total of 10 Cresyl violet-stained brain sections from each rat were selected at random from evenly spaced brain sections (Cheng et al., 2016).

2.9. Immunofluorescence

Immunofluorescence was carried out as described previously at room temperature (Zhao et al., 2015). The primary antibodies used were rabbit anti-Iba1 (microglial marker; 1:500; Wako Chemicals, Richmond, VA, USA) and rabbit anti-glial fibrillary acidic protein (GFAP, astrocyte marker; 1:500; Dako). Stained sections were examined under a fluorescence microscope (Eclipse TE2000-E, Nikon, Tokyo, Japan). Activated microglia and astrocytes were quantified on sections at 1.0, 1.7, and 2.5 mm from the bregma. Three sections per rat were viewed and photographed by an investigator blinded to group. The numbers of activated microglia and astrocytes over a 40 × microscopic field from 12 locations per rat (4 fields per section × 3 sections per rat) were averaged and expressed as positive cells per square millimeter (n = 5 rats per group) (Zhao et al., 2015). The ROI was defined within one 20x field that corresponded to 460 μm from the edge of the lesion.

2.10. Morphometric assessment of microglia and astrocytes

We used a computer-based tracing system (Neurolucida software, MicroBrightfield, Colchester, VT) (Niv et al., 2012) to trace and analyze dendrites and cell bodies of microglia and astrocytes in the peri-lesional APTw-hyperintense brain areas. We analyzed cell body area, cell volume, number of branches and trees, and total surface and length of dendrites for Iba1- and GFAP-positive cells on each immunofluorescence image under 40 × objective. We analyzed three to four cells per field from four fields per section and three sections per rat.

2.11. Statistical analysis

All results are presented as mean ± SD. The differences in all behavioral tests, lesion volumes, and MRI signal intensities in five ROIs between three groups (sham, TBI + vehicle, and TBI + pinocembrin groups) were assessed by a two-way repeated measures ANOVA. Absolute neuronal number and quantitative assessments of microglia and astrocytes were assessed by one-way ANOVA followed by post hoc test to detect differences between groups. The criterion for statistical significance was $P < 0.05$.

3. Results

In this study, the mortality of rats was 10% (2 of 20) in the vehicle group and 6% (1 of 16) in the pinocembrin-treated group. The three rats that died before the end of the study were excluded from the final data analysis.

3.1. Time course of multiparametric MRI in rats after TBI

We first performed a multiparametric MRI assessment on TBI lesions at 1 h and 1, 3, 7, 14, and 28 days post-TBI in the untreated (TBI + vehicle) group (n = 13; Fig. 1). At the earliest time point, the most noticeable change in MRI was observed in the CBF measurement. The average CBF values were significantly lower in the ipsilateral brain areas (central lesion, ipsilateral hippocampus, and ipsilateral cortex) than in the contralateral brain areas ($P < 0.001$). The decreased CBF signals in the perilesional areas could cause cerebral ischemia, leading to the decreased APTw signals (Fig. 1f). Notably, the CBF signals at 3 days post-TBI increased significantly in the ipsilateral perilesional areas, compared with those in the contralateral brain areas ($P < 0.0001$). Similarly, the APTw signals at 3 and 7 days post-TBI increased significantly in these ipsilateral perilesional areas ($P < 0.05$). As described below in sections on histopathology and immunofluorescence, these changes in CBF and APTw can be attributed to the inflammatory response, typically observed within a few weeks after TBI. The T_2, T_1, and ADC signals showed consistent increases over time, whereas the magnetization transfer ratio (MTR) decreased consistently in the ipsilateral brain areas (central lesion, ipsilateral hippocampus, and ipsilateral cortex) compared with those of the contralateral brain areas. Substantial changes in these four MRI parameters can be seen at 14 and 28 days post-TBI. Because the APTw MRI signal is sensitive to tissue pH, cellular mobile protein and peptide concentrations, and several other factors (Zhou et al., 2003, 2011), we observed more complex changes as a function of time by APTw than by other MRI techniques. We quantified the changes of these MRI parameters at 3 days post-TBI to assess the neuroprotection by pinocembrin (shown below).

3.2. Pinocembrin has cerebroprotective effects after TBI

We then administered pinocembrin to rats with TBI. We used T_2w MRI to measure lesion volume, and used the mNSS, beam walking, and rotarod tests to assess neurologic function at 1 h and 1, 3, 7, 14, and 28 days after TBI (n = 5 per group; Fig. 2). Lesion volumes varied with time after CCI and were largest at 3 days. Compared with the vehicle-treated group, rats that received 5 or 10 mg/kg pinocembrin exhibited significantly smaller lesion volumes beginning at 3 days post-TBI ($P < 0.05$ at each time point). They also had significantly lower mNSS ($P < 0.05$ at each time point) and performed better on the rotarod test ($P < 0.05$ at each time point) than did the vehicle-treated rats beginning at 3 days post-TBI. Additionally, from day 1 after CCI, pinocembrin-treated rats showed significantly better beam-walking ability than did the vehicle-treated rats ($P < 0.05$ at each time point).

3.3. Multiple MRI signals showed protective effects of pinocembrin

We assessed the changes in T_2, T_1, ADC, CBF, APTw, and MTR MRI signals at 3 days post-TBI (n = 5 per group; Fig. 3). At 3 days after TBI, the lesion became quite heterogeneous. In the lesion core, all MRI parameters (except T_2) were very similar in the vehicle-treated and pinocembrin-treated TBI groups. However, most of the MRI parameters revealed protection by pinocembrin in the surrounding areas (ipsilateral cortex and hippocampus). The ADC, CBF, and APTw signal intensities of both perilesional regions increased significantly in the vehicle-treated TBI group (all $P < 0.001$ vs. sham), but were significantly less intense in the pinocembrin-treated TBI group (all $P < 0.01$ vs. TBI + vehicle group). Notably, APTw MRI

showed dramatic and consistent changes in these surrounding areas. Also, in the surrounding areas, MTR was significantly decreased in the TBI + vehicle group (both $P < 0.001$ vs. sham) and significantly increased in the pinocembrin-treated TBI group (both $P < 0.05$ vs. TBI + vehicle).

3.4. Pinocembrin increased the number of surviving neurons

We used the stereology method to determine the number of surviving neurons in the perilesional region at 3 days after TBI (n = 5 per group; Fig. 4). Neurons with condensed (pyknotic) nuclei were considered dead or dying in the TBI brain. Rats in the TBI + vehicle group showed a large decrease in the number of surviving neurons, compared with that in the sham group. However, neuronal survival was significantly greater in the TBI group treated with 5 mg/kg pinocembrin than in the vehicle-treated TBI group ($P < 0.05$).

3.5. Pinocembrin decreased microglial activation

It is known that microglia and astrocytes are activated after TBI and contribute to early-stage brain injury. We used Iba1 and GFAP immunofluorescence labeling to examine the effect of pinocembrin treatment on microglial and astrocyte activation (n = 5; Fig. 5). Compared with resting microglia and astrocytes in the sham brain, reactive microglia and astrocytes in the perilesional region of the TBI + vehicle group exhibited more intense Iba1 and GFAP immunoreactivity and a greater number, length, and thickness of Iba1- and GFAP-positive processes. Pinocembrin treatment decreased the number of reactive microglia and astrocytes in the perilesional area on day 3 after TBI ($P < 0.05$), compared with that in the vehicle-treated TBI group.

3.6. Characterization of microglia and astrocytes in different groups

Finally, we characterized the morphology of microglia (Fig. 6) and astrocytes (Fig. 7) at 3 days after TBI with Neurolucida software (n = 5 per group). We counted 180–240 cells each in the sham group, TBI + vehicle group, and TBI + pinocembrin group. Microglia from the TBI + vehicle group showed significant increases in cell body area ($P < 0.0001$), cell volume ($P < 0.01$), number of dendrites ($P < 0.05$), total surface of dendrites ($P < 0.01$), total length of dendrites ($P < 0.05$), and number of branches (trees; $P < 0.0008$) compared with corresponding values of the sham group. Pinocembrin treatment significantly reversed those changes. Interestingly, astrocytes from the TBI + vehicle group exhibited significant increases only in cell body area ($P < 0.0008$) and number of branches ($P < 0.05$) compared with those of the sham group (n = 5 rats per group, $P < 0.05$). Pinocembrin significantly decreased cell body area compared with the vehicle treatment. These results indicate that microglia have the capacity to change their morphology more dramatically than astrocytes after TBI and that pinocembrin can inhibit microglial and astrocyte activation, thereby reducing secondary brain damage after TBI.

4. Discussion

TBI typically causes injury in two phases. In the primary phase, TBI causes direct damage to brain parenchyma, producing contusion, hemorrhage, and axonal injury. The secondary injury, caused by ischemia and inflammation, can be detected in the injury site and the

surrounding brain regions. The direct damage is almost impossible to treat. Therefore, preclinical and clinical researchers focus on the prevention, recognition, and treatment of secondary brain injury. The delayed secondary injury provides a window of opportunity to treat TBI and to improve functional outcomes (Lozano et al., 2015). As such, the brain tissue surrounding the impacted core is the focus of our research. To the best of our knowledge, this is the first study to use multiparameter MRI to assess TBI-induced secondary brain injury over time. We observed that CBF and APTw MRI signals were significantly increased in the perilesional areas of untreated TBI rats at 3 days post-TBI; these changes could be attributed to the increased glial response. Moreover, the time-dependent increases in ADC and decreases in MTR signals in untreated TBI rats were likely due to brain edema. We also found that post-treatment with pinocembrin decreased microglial/macrophage and astrocyte activation at 3 days, consistent with the recovery of the CBF and APTw MRI signals in the secondary injury regions. These findings provide clear evidence that pinocembrin is cerebroprotective for TBI and that multiple MRI signals, particularly CBF and APTw, are sensitive biomarkers for assessment of neuroinflammation and drug efficacy after TBI.

One important finding from this study was that the structural MRI parameters (T_2 and T_1), which are routinely used in the clinic, were not sufficiently sensitive for detection of abnormalities after TBI. These results are consistent with those of a previous study (Talley Watts et al., 2015). By contrast, functional MRI (ADC and CBF) and molecular MRI (APTw and MTR) exhibited more sensitivity to detect secondary brain injury than did conventional structural MRI. Changes in signal intensities of ADC, CBF, and MTR have been reported previously in animal models of TBI (Li et al., 2016; Maegele et al., 2015; Tu et al., 2016). In particular, it was found that changes in the ADC values early after TBI correlate with brain tissue ATP content (Maegele et al., 2015). In our study, ADC values in the core area and in the perilesional ROI brain regions increased consistently from day 3 to day 28, indicative of vasogenic edema (Frey et al., 2014; Nakasu et al., 1995). Changes in the MTR signal intensity showed an opposite trend. A prior study reported a similar change in the ADC values in the perilesional ROI regions but a different trend in the core area (Wei et al., 2012). The difference may result from different models used (CCI model vs. weight-drop model). We further found that the elevated ADC values in the perilesional regions can be reduced by pinocembrin treatment on day 3 post-TBI. Notably, CBF and APTw signals were consistently and markedly increased in the ipsilateral perilesional areas on day 3 post-TBI, compared to those in the corresponding contralateral brain region, but pinocembrin reduced this effect. In several previous studies, researchers found that pinocembrin had neuroprotective effects against cerebral ischemia *in vivo* and *in vitro* (Guang and Du, 2006; Liu et al., 2008; Wu et al., 2013). In our study, we found that pinocembrin post-treatment decreased brain lesion volume, increased the number of surviving neurons, and improved neurologic function (motor, sensory, reflex, and balance) after TBI and that the neuroprotective effects were associated with inhibition of microglial/macrophage and astrocyte activation based on cell number and morphology. Our data indicate that pinocembrin reduces vasogenic edema and reverses the increase in CBF that is probably induced by inflammatory response.

The APT-MRI technique has recently gained special attention as a way to assess various brain diseases and their response to therapy (Zhou et al., 2003, 2011). APT imaging is an

important molecular MRI technique that can generate contrast based on tissue pH (Jin et al., 2012; Sun et al., 2007; Tietze et al., 2014; Zhou and van Zijl, 2011) or concentrations of endogenous mobile proteins and peptides (Jiang et al., 2016; Yan et al., 2015; Zhou et al., 2013). The most important novel finding of this study was that APTw signals increased significantly in the perilesional brain regions of untreated TBI rats at 3 and 7 days. Furthermore, pinocembrin treatment was able to reduce the increased APTw signals. The recovery from increased APTw MRI signals correlated with decreased microglial/macrophage and astrocyte activation in the same secondary injury regions. These results suggest that increased APTw signals might result from the increased secondary inflammatory response, which might lead to increases in mobile protein. A marked synchronous change in the inflammatory cells and APTw signals indicates to us that APTw MRI could be a sensitive biomarker for neuroinflammation (Loane and Faden, 2010; Wang et al., 2013b).

In conclusion, our early data show that pinocembrin treatment has a cerebroprotective effect in the CCI-TBI model in rats. Moreover, multiple MRI signals, CBF and APTw in particular, have great potential as unique, sensitive imaging biomarkers for the identification of secondary brain injury caused by CBF reduction, brain edema, and inflammatory response and for the assessment of drug efficacy in the TBI model.

Acknowledgments

We thank Claire Levine for assistance with this manuscript. This work was supported by grants from the American Heart Association (13GRNT15730001), the National Institutes of Health (R01AT007317, R01NS078026, R01EB009731, R01CA166171, R01NS083435), and a “Stimulating and Advancing ACCM Research (StAAR)” grant from the Department of Anesthesiology and Critical Care Medicine, Johns Hopkins University. Wenzhu Wang is the recipient of the China Scholarship Council Joint PhD Training award (CSC NO. 201406370078).

Abbreviations

APTw MRI	amide proton transfer-weighted MRI
CBF	cerebral blood flow
CCI	controlled cortical impact
TE	echo time
GFAP	glial fibrillary acidic protein
mNSS	modified neurologic severity score
MRI	magnetic resonance imaging
MTR	magnetization transfer ratio
ROI	region of interest
rpm	revolutions per minute
TBI	traumatic brain injury

TR repetition time

References

Amyot F, Arciniegas DB, Brazaitis MP, Curley KC, Diaz-Arrastia R, Gandjbakhche A, Herscovitch P, Hinds SR 2nd, Manley GT, Pacifico A, Razumovsky, Riley J, Salzer W, Shih R, Smirniotopoulos JG, Stocker D. A review of the effectiveness of neuroimaging modalities for the detection of traumatic brain injury. J Neurotrauma. 2015; 32:1693–1721. [PubMed: 26176603]

Cao G, Ying P, Yan B, Xue W, Li K, Shi A, Sun T, Yan J, Hu X. Pharmacokinetics, safety, and tolerability of single and multiple-doses of pinocembrin injection administered intravenously in healthy subjects. J Ethnopharmacol. 2015; 168:31–36. [PubMed: 25814318]

Cheng T, Wang W, Li Q, Han X, Xing J, Qi C, Lan X, Wan J, Potts A, Guan F, Wang J. Cerebroprotection of flavanol (-)-epicatechin after traumatic brain injury via Nrf2-dependent and -independent pathways. Free Radic Biol Med. 2016; 92:15–28. [PubMed: 26724590]

de Oliveira, MR., Peres, A., Gama, CS., Bosco, SM. Pinocembrin provides mitochondrial protection by the activation of the Erk1/2-Nrf2 signaling pathway in SH-SY5Y neuroblastoma cells exposed to paraquat. Mol Neurobiol. 2016. http://dx.doi.org/10.1007/s12035-12016-10135-12035. in press

Frey L, Lepkin A, Schickedanz A, Huber K, Brown MS, Serkova N. ADC mapping and T1-weighted signal changes on post-injury MRI predict seizure susceptibility after experimental traumatic brain injury. Neurol Res. 2014; 36:26–37. [PubMed: 24107461]

Goldstein LB, Davis JN. Beam-walking in rats: studies towards developing an animal model of functional recovery after brain injury. J Neurosci Methods. 1990; 31:101–107. [PubMed: 2319810]

Guang HM, Du GH. Protections of pinocembrin on brain mitochondria contribute to cognitive improvement in chronic cerebral hypoperfused rats. Eur J Pharmacol. 2006; 542:77–83. [PubMed: 16806158]

Hamm RJ, Pike BR, O'Dell DM, Lyeth BG, Jenkins LW. The rotarod test: an evaluation of its effectiveness in assessing motor deficits following traumatic brain injury. J Neurotrauma. 1994; 11:187–196. [PubMed: 7932797]

Han X, Lan X, Li Q, Gao Y, Zhu W, Cheng T, Maruyama T, Wang J. Inhibition of prostaglandin E2 receptor EP3 mitigates thrombin-induced brain injury. J Cereb Blood Flow Metab. 2016; 36:1059–1074. [PubMed: 26661165]

Jaiswal MK. Toward a high-resolution neuroimaging biomarker for mild traumatic brain injury: from bench to bedside. Front Neurol. 2015; 6:148. [PubMed: 26217296]

Jiang S, Yu H, Wang X, Lu S, Li Y, Feng L, Zhang Y, Heo HY, Lee DH, Zhou J, Wen Z. Molecular MRI differentiation between primary central nervous system lymphomas and high-grade gliomas using endogenous protein-based amide proton transfer MR imaging at 3 Tesla. Eur Radiol. 2016; 26:64–71. [PubMed: 25925361]

Jin T, Wang P, Zong X, Kim SG. Magnetic resonance imaging of the Amine-Proton EXchange (APEX) dependent contrast. Neuroimage. 2012; 59:1218–1227. [PubMed: 21871570]

Kapoor S. Comment on isolation and identification of compounds from Penthorum chinense Pursh with antioxidant and antihepatocarcinoma properties: pinocembrin and its rapidly emerging neuroprotective effects. J Agric Food Chem. 2013; 61:1416. [PubMed: 23305216]

Lan X, Wang W, Li Q, Wang J. The natural flavonoid pinocembrin: molecular targets and potential therapeutic applications. Mol Neurobiol. 2016; 53:1794–1801. [PubMed: 25744566]

Lan X, Han X, Li Q, Li Q, Gao Y, Cheng T, Wan J, Zhu W, Wang J. Pinocembrin protects hemorrhagic brain primarily by inhibiting toll-like receptor 4 and reducing M1 phenotype microglia. Brain Behav Immun. 2017; 61:326–339. [PubMed: 28007523]

Li W, Watts L, Long J, Zhou W, Shen Q, Jiang Z, Li Y, Duong TQ. Spatiotemporal changes in blood-brain barrier permeability, cerebral blood flow, T2 and diffusion following mild traumatic brain injury. Brain Res. 2016; 1646:53–61. [PubMed: 27208495]

Liu R, Gao M, Yang ZH, Du GH. Pinocembrin protects rat brain against oxidation and apoptosis induced by ischemia-reperfusion both in vivo and in vitro. Brain Res. 2008; 1216:104–115. [PubMed: 18495093]

Liu R, Li JZ, Song JK, Zhou D, Huang C, Bai XY, Xie T, Zhang X, Li YJ, Wu CX, Zhang L, Li L, Zhang TT, Du GH. Pinocembrin improves cognition and protects the neurovascular unit in Alzheimer related deficits. Neurobiol Aging. 2014; 35:1275–1285. [PubMed: 24468471]

Loane DJ, Faden AI. Neuroprotection for traumatic brain injury: translational challenges and emerging therapeutic strategies. Trends Pharmacol Sci. 2010; 31:596–604. [PubMed: 21035878]

Long JA, Watts LT, Li W, Shen Q, Muir ER, Huang S, Boggs RC, Suri A, Duong TQ. The effects of perturbed cerebral blood flow and cerebrovascular reactivity on structural MRI and behavioral readouts in mild traumatic brain injury. J Cereb Blood Flow Metab. 2015; 35:1852–1861. [PubMed: 26104285]

Lozano D, Gonzales-Portillo GS, Acosta S, de la Pena I, Tajiri N, Kaneko Y, Borlongan CV. Neuroinflammatory responses to traumatic brain injury: etiology, clinical consequences, and therapeutic opportunities. Neuropsychiatr Dis Treat. 2015; 11:97–106. [PubMed: 25657582]

Maegele M, Stuermer EK, Hoeffgen A, Uhlenkueken U, Mautes A, Schaefer N, Lippert-Gruener M, Schaefer U, Hoehn M. Multimodal MR imaging of acute and subacute experimental traumatic brain injury: Time course and correlation with cerebral energy metabolites. Acta Radiol Short Rep. 2015; 4 2047981614555142.

Mao W, Schuler MA, Berenbaum MR. Honey constituents up-regulate detoxification and immunity genes in the western honey bee Apis mellifera. Proc Natl Acad Sci U S A. 2013; 110:8842–8846. [PubMed: 23630255]

McConeghy KW, Hatton J, Hughes L, Cook AM. A review of neuroprotection pharmacology and therapies in patients with acute traumatic brain injury. CNS Drugs. 2012; 26:613–636. [PubMed: 22668124]

Meng F, Wang Y, Liu R, Gao M, Du G. Pinocembrin alleviates memory impairment in transient global cerebral ischemic rats. Exp Ther Med. 2014; 8:1285–1290. [PubMed: 25187841]

Nakasu Y, Nakasu S, Morikawa S, Uemura S, Inubushi T, Handa J. Diffusion-weighted MR in experimental sustained seizures elicited with kainic acid. AJNR Am J Neuroradiol. 1995; 16:1185–1192. [PubMed: 7677009]

Niv F, Keiner S, Krishna, Witte OW, Lie DC, Redecker C. Aberrant neurogenesis after stroke: a retroviral cell labeling study. Stroke. 2012; 43:2468–2475. [PubMed: 22738919]

Rasul A, Millimouno FM, Ali Eltayb W, Ali M, Li J, Li X. Pinocembrin: a novel natural compound with versatile pharmacological and biological activities. Biomed Res Int. 2013; 2013:379850. [PubMed: 23984355]

Saad MA, Abdel Salam RM, Kenawy SA, Attia AS. Pinocembrin attenuates hippocampal inflammation, oxidative perturbations and apoptosis in a rat model of global cerebral ischemia reperfusion. Pharmacol Rep. 2015; 67:115–122. [PubMed: 25560584]

Sayre CL, Alrushaid S, Martinez SE, Anderson HD, Davies NM. Pre-clinical pharmacokinetic and pharmacodynamic characterization of selected chiral flavonoids: pinocembrin and pinostrobin. J Pharm Pharm Sci. 2015; 18:368–395. [PubMed: 26626242]

Shi LL, Chen BN, Gao M, Zhang HA, Li YJ, Wang L, Du GH. The characteristics of therapeutic effect of pinocembrin in transient global brain ischemia/reperfusion rats. Life Sci. 2011; 88:521–528. [PubMed: 21262238]

Shultz SR, Wright DK, Zheng P, Stuchbery R, Liu SJ, Sashindranath M, Medcalf RL, Johnston LA, Hovens CM, Jones NC, O'Brien TJ. Sodium selenate reduces hyperphosphorylated tau and improves outcomes after traumatic brain injury. Brain. 2015; 138:1297–1313. [PubMed: 25771151]

Sun PZ, Zhou J, Sun W, Huang J, van Zijl PC. Detection of the ischemic penumbra using pH-weighted MRI. J Cereb Blood Flow Metab. 2007; 27:1129–1136. [PubMed: 17133226]

Talley Watts L, Shen Q, Deng S, Chemello J, Duong TQ. Manganese-enhanced magnetic resonance imaging of traumatic brain injury. J Neurotrauma. 2015; 32:1001–1010. [PubMed: 25531419]

Tietze A, Blicher J, Mikkelsen IK, Ostergaard L, Strother MK, Smith SA, Donahue MJ. Assessment of ischemic penumbra in patients with hyperacute stroke using amide proton transfer (APT) chemical exchange saturation transfer (CEST) MRI. NMR Biomed. 2014; 27:163–174. [PubMed: 24288260]

Tu TW, Williams RA, Lescher JD, Jikaria N, Turtzo LC, Frank JA. Radiological-pathological correlation of diffusion tensor and magnetization transfer imaging in a closed head traumatic brain injury model. Ann Neurol. 2016; 79:907–920. [PubMed: 27230970]

Wang J, Yu L, Jiang C, Chen M, Ou C, Wang J. Bone marrow mononuclear cells exert long-term neuroprotection in a rat model of ischemic stroke by promoting arteriogenesis and angiogenesis. Brain Behav Immun. 2013a; 34:56–66. [PubMed: 23891963]

Wang G, Zhang J, Hu X, Zhang L, Mao L, Jiang X, Liou AK, Leak RK, Gao Y, Chen J. Microglia/macrophage polarization dynamics in white matter after traumatic brain injury. J Cereb Blood Flow Metab. 2013b; 33:1864–1874. [PubMed: 23942366]

Wang M, Hong X, Chang CF, Li Q, Ma B, Zhang H, Xiang S, Heo HY, Zhang Y, Lee DH, Jiang S, Leigh R, Koehler RC, van Zijl PC, Wang J, Zhou J. Simultaneous detection and separation of hyperacute intracerebral hemorrhage and cerebral ischemia using amide proton transfer MRI. Mag Reson Med. 2015; 74:42–50.

Wang W, Li H, Yu J, Hong M, Zhou J, Zhu L, Wang Y, Luo M, Xia Z, Yang ZJ, Tang T, Ren P, Huang X, Wang J. Protective effects of Chinese herbal medicine Rhizoma drynariae in rats after traumatic brain injury and identification of active compound. Mol Neurobiol. 2016a; 53:4809–4820. [PubMed: 26334614]

Wang Y, Miao Y, Mir AZ, Cheng L, Wang L, Zhao L, Cui Q, Zhao W, Wang H. Inhibition of beta-amyloid-induced neurotoxicity by pinocembrin through Nrf2/HO-1 pathway in SH-SY5Y cells. J Neurol Sci. 2016b; 368:223–230. [PubMed: 27538638]

Wei XE, Zhang YZ, Li YH, Li MH, Li WB. Dynamics of rabbit brain edema in focal lesion and perilesion area after traumatic brain injury: a MRI study. J Neurotrauma. 2012; 29:2413–2420. [PubMed: 21675826]

Wu CX, Liu R, Gao M, Zhao G, Wu S, Wu CF, Du GH. Pinocembrin protects brain against ischemia/reperfusion injury by attenuating endoplasmic reticulum stress induced apoptosis. Neurosci Lett. 2013; 546:57–62. [PubMed: 23669639]

Yan B, Cao G, Sun T, Zhao X, Hu X, Yan J, Peng Y, Shi A, Li Y, Xue W, Li M, Li K, Liu Y. Determination of pinocembrin in human plasma by solid-phase extraction and LC/MS/MS: application to pharmacokinetic studies. Biomed Chromatogr. 2014; 28:1601–1606. [PubMed: 24733513]

Yan K, Fu Z, Yang C, Zhang K, Jiang S, Lee DH, Heo HY, Zhang Y, Cole RN, Van Eyk JE, Zhou J. Assessing amide proton transfer (APT) MRI contrast origins in 9 L gliosarcoma in the rat brain using proteomic analysis. Mol Imaging Biol. 2015; 17:479–487. [PubMed: 25622812]

Yang ZJ, Wang B, Kwansa H, Heitmiller KD, Hong G, Carter EL, Jamrogowicz JL, Larson AC, Martin LJ, Koehler RC. Adenosine A2A receptor contributes to ischemic brain damage in newborn piglet. J Cereb Blood Flow Metab. 2013; 33:1612–1620. [PubMed: 23860373]

Yang J, Li Q, Wang Z, Qi C, Han X, Lan X, Wan J, Wang W, Zhao X, Hou Z, Gao C, Carhuapoma JR, Mori S, Zhang J, Wang J. Multimodality MRI assessment of grey and white matter injury and blood-brain barrier disruption after intracerebral haemorrhage in mice. Sci Rep. 2017; 7:40358. [PubMed: 28084426]

Zhao X, Wu T, Chang CF, Wu H, Han X, Li Q, Gao Y, Li Q, Hou Z, Maruyama T, Zhang J, Wang J. Toxic role of prostaglandin E2 receptor EP1 after intracerebral hemorrhage in mice. Brain Behav Immun. 2015; 46:293–310. [PubMed: 25697396]

Zhou J, van Zijl PC. Defining an acidosis-based ischemic penumbra from pH-weighted MRI. Transl Stroke Res. 2011; 3:76–83. [PubMed: 22408691]

Zhou J, Payen JF, Wilson DA, Traystman RJ, van Zijl PC. Using the amide proton signals of intracellular proteins and peptides to detect pH effects in MRI. Nat Med. 2003; 9:1085–1090. [PubMed: 12872167]

Zhou J, Tryggestad E, Wen Z, Lal B, Zhou T, Grossman R, Wang S, Yan K, Fu DX, Ford E, Tyler B, Blakeley J, Laterra J, van Zijl PC. Differentiation between glioma and radiation necrosis using molecular magnetic resonance imaging of endogenous proteins and peptides. Nat Med. 2011; 17:130–134. [PubMed: 21170048]

Zhou J, Zhu H, Lim M, Blair L, Quinones-Hinojosa A, Messina SA, Eberhart CG, Pomper MG, Laterra J, Barker PB, van Zijl PC, Blakeley JO. Three-dimensional amide proton transfer MR

imaging of gliomas: Initial experience and comparison with gadolinium enhancement. J Magn Reson Imaging. 2013; 38:1119–1128. [PubMed: 23440878]

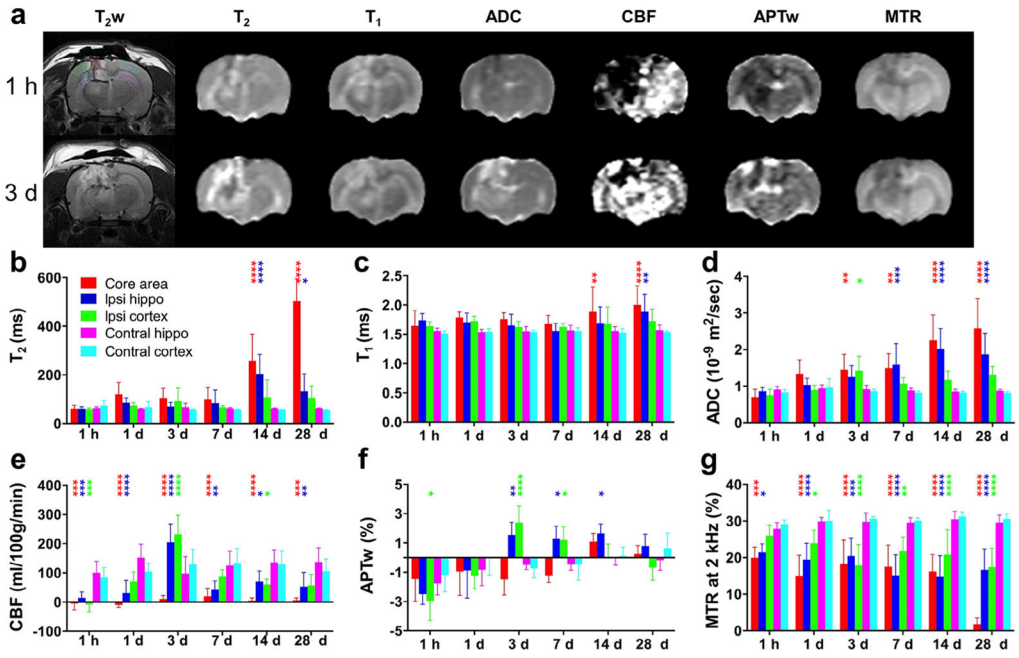

Fig. 1.

Quantitative multiparametric MRI assessment of traumatic brain injury (TBI) in rats. (a) Representative multiparametric MRI images in a rat at 1 h and 3 days after TBI. The five regions of interest (ROIs) are marked by dotted lines on the upper left T_2-weighted (T_2w) image. (b–g) Plots of MRI signal intensities in all five ROIs, acquired at 1 h and 1, 3, 7, 14, and 28 days after TBI (n = 13). All MRI parameters were sensitive for detecting TBI at some time points. Notably, APTw and CBF MRI showed relatively large changes at 3 days post-TBI in ipsilateral perilesional areas, compared with those in corresponding contralateral brain areas. $^{*}P < 0.05$, $^{**}P < 0.01$, $^{***}P < 0.001$, $^{****}P < 0.0001$ versus the corresponding contralateral brain areas.

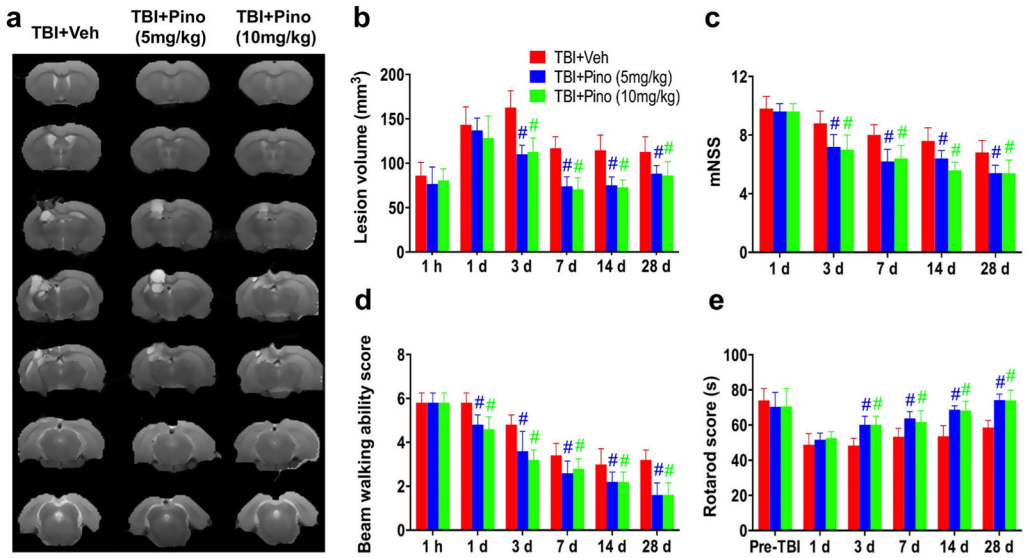

Fig. 2.

Neuroprotection by pinocembrin in rats with traumatic brain injury (TBI). (a, b) T_2-weighted (T_2w) images for all seven slices at 28 days post-TBI and the lesion volumes at indicated time points for the TBI + vehicle and TBI + pinocembrin groups (n = 5 per group). TBI rats treated with pinocembrin (5 and 10 mg/kg) had smaller lesion volumes at 3, 7, 14, and 28 days after TBI than did rats in the TBI + vehicle group. (c–e) Behavioral testing results from the modified neurologic severity score (mNSS), beam walking, and rotarod tests. Compared with the vehicle-treated TBI group, the two pinocembrin-treated TBI groups had better neurologic function at 1 (for beam walking only), 3, 7, 14, and 28 days post-TBI. $^{\#}P < 0.05$ versus the TBI + vehicle group.

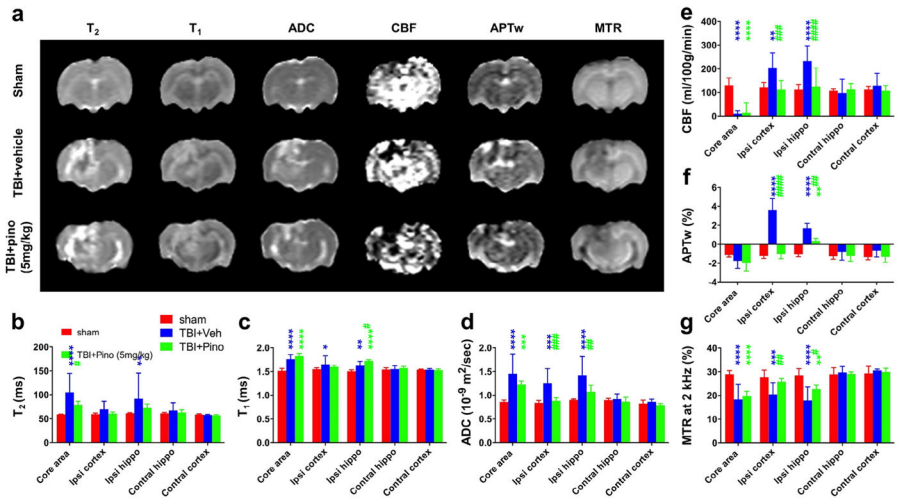

Fig. 3.

Quantitative multiparametric MRI assessment of neuroprotection by pinocembrin in rats with traumatic brain injury (TBI). (a) Representative images of multiparametric MRI signals at 3 days post-TBI in sham, TBI + vehicle, and TBI + pinocembrin (pino; 5 mg/kg) groups (n = 5 per group). Notably, the TBI lesion became heterogeneous with areas of high and low APTw signal intensities. The APTw signal intensity of the perilesional region increased dramatically in the vehicle-treated TBI rats, but less so in the pinocembrin-treated TBI rats. The ADC, which probes the diffusion rate of water molecules, had a significantly lower signal in the pinocembrin-treated TBI rats than in the vehicle-treated TBI rats. The CBF signal showed a similar trend with pinocembrin treatment. (b–g) Quantitative analysis of multiparametric MRI signal intensities in five regions of interest (ROIs). In general, the ADC, CBF, and APTw MRI signals in surrounding areas (ipsilateral cortex and hippocampus) showed significant increases in the vehicle-treated TBI group that were ameliorated in the pinocembrin-treated TBI group. Conversely, the MTR showed a significant decrease in the vehicle-treated TBI group that was reversed by pinocembrin treatment. $^{*}P < 0.05$, $^{**}P < 0.01$, $^{***}P < 0.001$, $^{****}P < 0.0001$ compared with the sham group; $^{\#}P < 0.05$, $^{\#\#}P < 0.01$, $^{\#\#\#}P < 0.001$, $^{\#\#\#\#}P < 0.0001$ compared with the vehicle-treated TBI group.

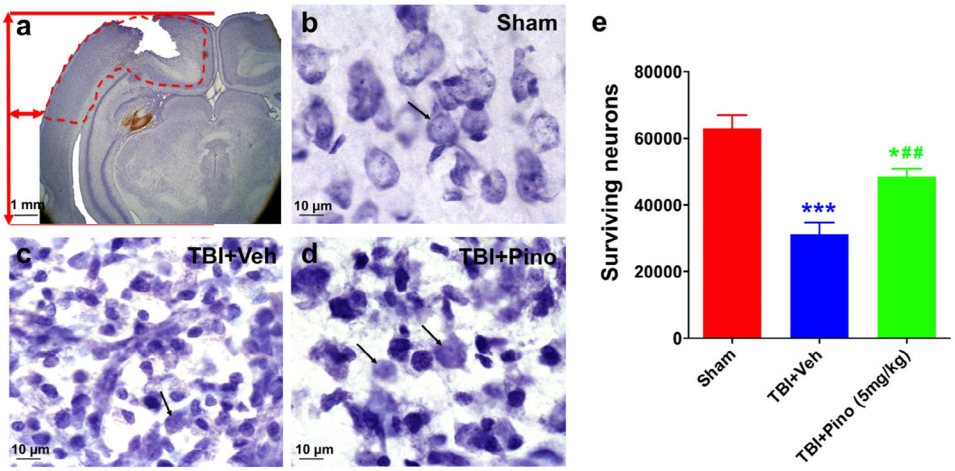

Fig. 4.

Cresyl violet staining and stereological quantification of surviving neurons at 3 days after traumatic brain injury (TBI) in rats. (a) Representative Cresyl violet-stained brain sections from rats after TBI. The location in the ipsilateral cortex used to quantify the number of surviving neurons by stereology is delineated by a dashed red line. (b–d) Morphologic changes in cortical neurons after TBI. Sham brain showed healthy neurons, with large nuclei and distinct nucleoli, indicated by black arrows (b). TBI brain showed profound neuronal degeneration as indicated by the neuronal shrinkage and pyknotic nuclei (c). With pinocembrin treatment, many neurons exhibited normal appearance, but shrunken cells with pyknotic nuclei were still evident (d). (e) Volumetric density of viable neurons assessed in ipsilateral cortex by unbiased stereology (n = 5 per group). The TBI + vehicle group showed a significant decrease in viable neurons, compared with the sham group ($^{***}P < 0.001$). Importantly, rats treated with pinocembrin had significantly more viable neurons than did those treated with vehicle ($^{\#\#}P < 0.01$), although the number was still less than that of the sham group ($^{*}P < 0.05$). Scale bar in (a), 1 mm; scale bar in (b–d): 10 μm.

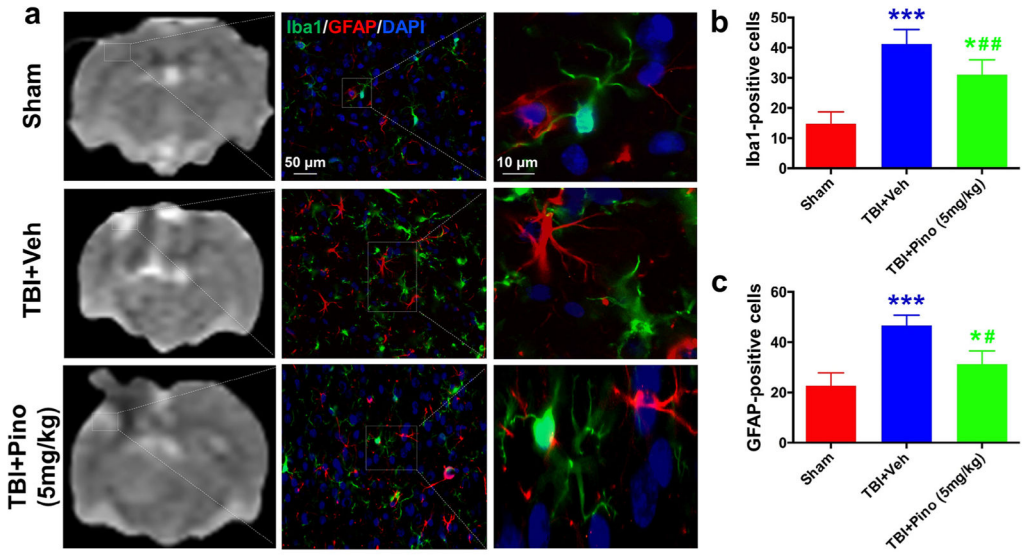

Fig. 5.

Glial response in the perilesional hyperintense brain areas at 3 days after traumatic brain injury (TBI) in rats. (a) APTw images and immunofluorescence labeling of microglia (Iba1, green) and astrocytes (GFAP, red) in rat brains from the sham, TBI + vehicle, and TBI + pinocembrin groups at 3 days post-TBI. Consistent with the changes to APTw signal in the perilesional region, at 3 days after TBI, fluorescence intensities of Iba1 and GFAP were significantly higher in the vehicle-treated TBI group than in the sham group. However, pinocembrin moderated the level of increase. (b, c) Quantitative analysis of Iba1-positive reactive microglia and GFAP-positive reactive astrocytes in the hyperintense surrounding areas (n = 5 per group). The TBI + vehicle group had greater numbers of Iba1- and GFAP-positive reactive cells than did the sham group ($^{***}P < 0.001$). The TBI + pinocembrin group had significantly fewer Iba1- and GFAP-positive reactive cells than did the TBI + vehicle group ($^{\#}P < 0.05$, $^{\#\#}P < 0.01$), but still had more than the sham group ($^{*}P < 0.05$). The data suggest that changes in the APTw signals may be associated with microglial and astrocyte activation. Scale bars in (a) middle column, 50 μm; right column, 10 μm.

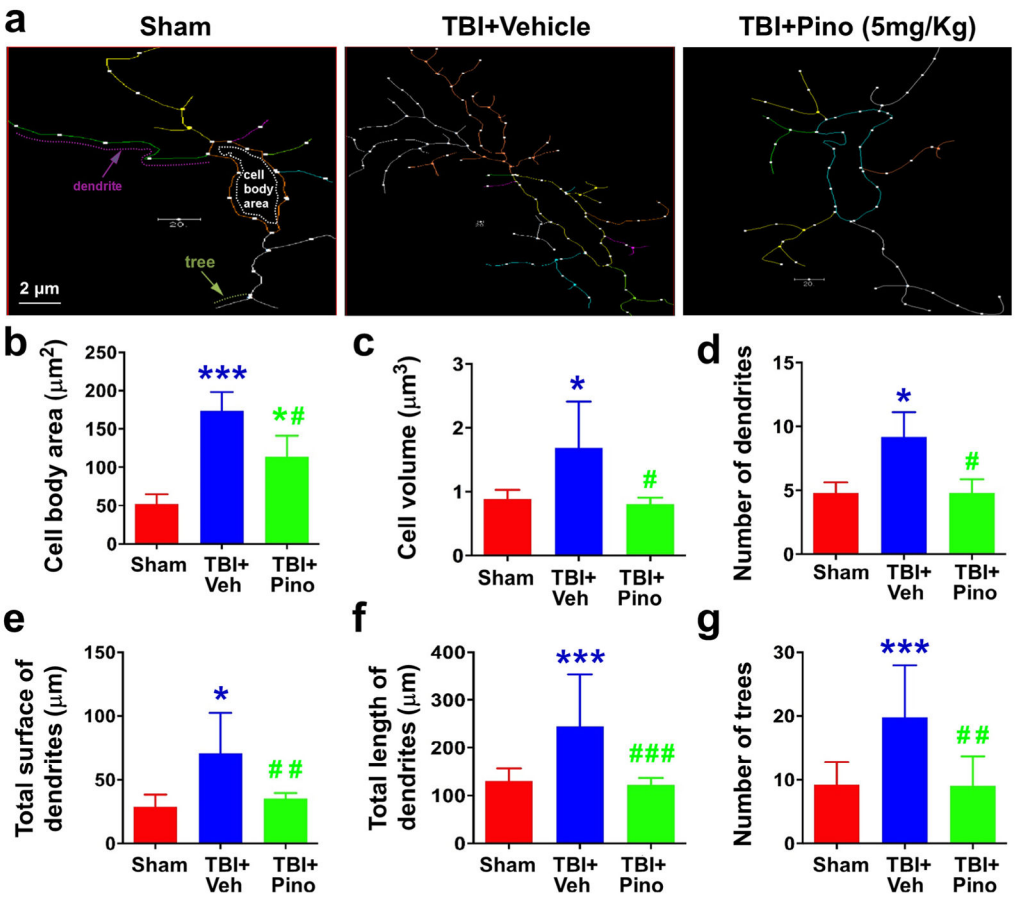

Fig. 6.

Morphometric assessment of microglia in the APTw-hyperintense areas of sham, TBI + vehicle, and TBI + pinocembrin groups (n = 5 per group). We used Neurolucida software, a computer-based tracing system, to trace and analyze the structure (dendrites and cell bodies) of microglia under a 40 × objective. (a) The traced images. (b–g) Changes in cell body area, cell volume, number of dendrites and trees, and total surface and length of dendrites. Cell body area of the microglia was greater in the TBI + vehicle group than in the sham group. Although, microglia in the TBI + pinocembrin group had significantly smaller cell bodies than microglia in the TBI + vehicle group, they remained larger than those in the sham group. Similarly, microglia in the TBI + vehicle group exhibited greater cell volume and total surface of dendrites, greater numbers of dendrites and trees, and longer dendrites than those of the sham groups, and pinocembrin treatment reversed these changes. Scale bars in (a): 2 μm. $^{*}P < 0.05$, $^{***}P < 0.001$ vs. sham; $^{\#}P < 0.05$ vs. TBI + vehicle.

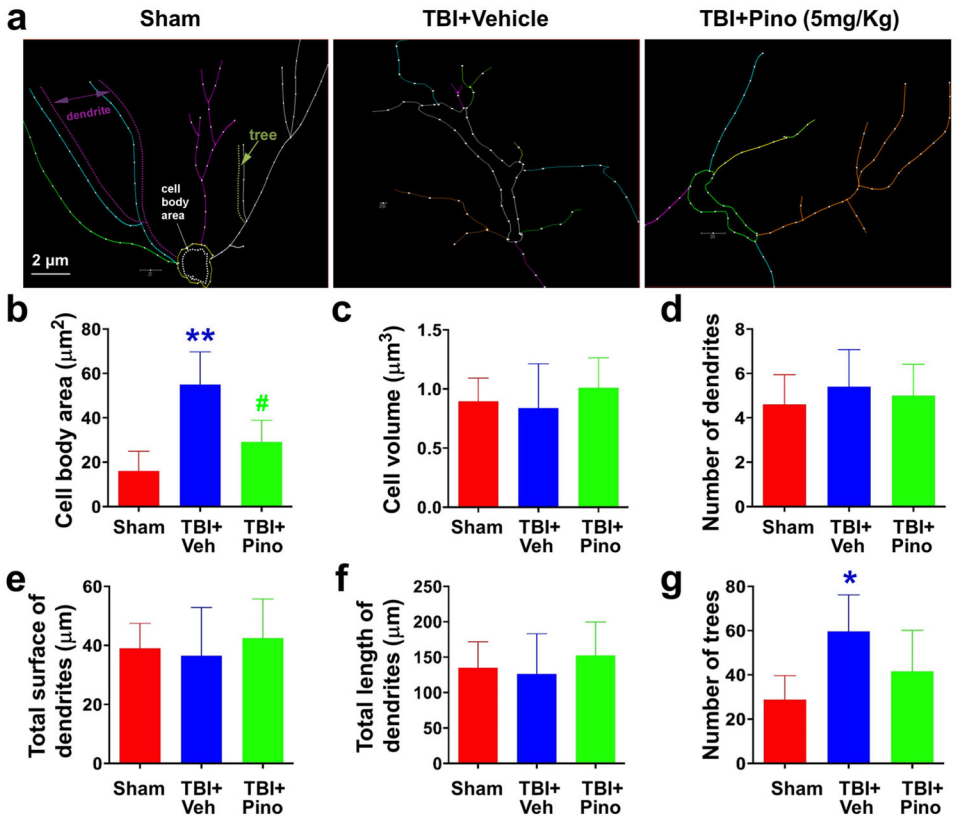

Fig. 7.

Morphometric assessment of astrocytes in the APTw-hyperintense areas of sham, TBI + vehicle, and TBI + pinocembrin groups (n = 5 per group). Neurolucida software was used to trace and analyze the structure (dendrites and cell bodies) of astrocytes. (a) The traced images. (b–g) Changes in cell body area, cell volume, number of dendrites and trees, and total surface and length of astrocytes. Cell body area of the three groups differed significantly. Astrocytes in the TBI + vehicle group had significantly greater cell body area than did astrocytes in the sham group, but pinocembrin mitigated the size increase. Astrocytes in the TBI + vehicle group displayed more trees than did astrocytes in the sham group, but the number was not reduced by pinocembrin. Scale bars in (a): 2 μm. $^{*}P < 0.05$, $^{**}P < 0.001$ versus sham; $^{\#}P < 0.05$ versus TBI + vehicle.